Optimal Operations of Nuclear-based Integrated Energy Systems with Mixed-Integer Programming

Jianqiao Huang, Binghui Li, Bikash Poudel
Idaho National Laboratory
Idaho Falls, ID, USA
{Jianqiao.Huang, binghui.li, Bikash.Poudel}@inl.gov

Jie Zhang
The University of Texas at Dallas
Richardson, TX, USA
jiezhang@utdallas.edu

Abstract—A nuclear-based integrated energy system (IES), consisting of multiple carbon-free energy generation and conversion technologies to meet heterogeneous end-use demands, offers a promising approach to decarbonize the U.S. economy. Operating such an IES is challenging due to its complexity and the diverse end-use demands, such as heating and electricity. This paper aims to address the optimal operation of an IES composed of a small modular reactor, a steam manifold, a balance of plant, a high-temperature steam electrolysis system, a district heating (DH) network, and electrical grids. We formulate the system's operation as a mixed-integer linear programming problem to maximize net revenues from sales of electricity and hydrogen. To evaluate the efficacy of the proposed model, we conduct a 24-hour simulation considering day-ahead electricity prices from the California Independent System Operator (CAISO) and a varying DH demand profile with hourly resolution. The simulation results show that our model effectively optimizes the operation by selling electricity during on-peak periods and purchasing electricity for hydrogen production during off-peak periods, while satisfying operating constraints within the IES.

Index Terms—Integrated energy system, cascade heat utilization, mixed-integer linear programming, small modular reactor

NOMENCLATURE

Indices

t	Index of time periods.

Variables

$\dot{m}_t^{BOP/HTSE/DH}$	Mass flow rate of steam distributed by steam manifold to BOP/HTSE/DH, kg/s.
$\dot{m}_t^{BV}$	Mass flow rate of steam bypassed to condenser using a turbine bypass valve, kg/s.
$\dot{m}_t^{c/d}$	Mass flow rate of the charging/discharging steam of TES, kg/s.
$\dot{m}_t^{H_2}$	Hydrogen production rate, kg/s.
$\dot{m}_t^{HX1/Tur}$	Mass flow rate of steam that enters heat exchanger 1 (HX1)/turbine, kg/s.
$h_t^{HTSE,ext}$	Specific enthalpy of steam that exits the heat exchanger of HTSE, kJ/kg.
p_t^g	Electric power output of BOP, kW.
p_t^{HTSE}	Electrical power consumed by HTSE, kWe.
p_t^{mech}	Mechanical power, kW.
$p_t^{s/b}$	Electrical power sold to/bought from grid, kWe.
$T_t^{N_3}$	Temperature of the DH working fluid before entering HX1, °C.
T_t^{TES}	Temperature of TES storage medium, °C.

Parameters

Δt	Simulation time step, s.
$\dot{m}_{max}^{c/d}$	Maximum charging/discharging flow rate, kg/s.
$\dot{m}_t^{CS}$	Steam delivered from SMR to the steam manifold, kg/s.
$\dot{m}_t^{pipe}$	Mass flow rate of DH supply water, kg/s.
$\eta_{t/g}$	Turbine/generator efficiency.
$a_{1,t}$	Electricity price, \$/kWh.
$a_{2,t}$	Hydrogen price, \$/kg.
$c^{p/str}$	Specific heat capacity of the DH working fluid/TES storage medium, kJ/(kg · K).
h^{CS}	Specific enthalpy of working fluid that exits the steam generator, kJ/kg.
$h_t^{Tur/DH,ext}$	Specific enthalpy of steam that exits the turbine/heat exchanger of DH, kJ/kg.
m^{str}	Mass of the TES storage medium, kg.
q_t^{dem}	Heat demand, kWth.
$T^{DH,in/out}$	Temperature of working fluid that exits/enters the DH, °C.
$T_{max/min}^{TES}$	Maximum/minimum temperature requirements of TES, °C.

I. INTRODUCTION

Nuclear-based integrated energy systems have received increasing attention recently. A nuclear-based integrated energy system (IES) typically consists of one or more nuclear reactors, renewable energy sources, and energy storage systems that are customized to meet multiple end-use demands [1], such as desalination, chemical manufacturing, hydrogen production, and district heating (DH) [2]–[7]. It is a cost-effective way to provide clean, reliable electricity and heat that can be used to decarbonize many hard-to-decarbonize energy sectors.

Optimization of the scheduling and operations of an IES are needed to maximize its economic performance. Such operation models can be found in many previous studies, such as distributed energy systems, home energy management systems, and wholesale electricity markets [8]–[10]. Most of these studies, however, only consider a single form of energy carrier, whereas multiple forms of energy carriers exist in an IES. Operating such a complex system, therefore, can be challenging because unlike electricity, temperature requirements

differ with different heat processes [11]–[13]. Careful design and scheduling are therefore a necessity.

In addition, one main challenge formulating the operations of IES is handling the conversion of different energy carriers and output products. In real world, these relationships are typically highly non-linear, whereas most previous studies assume linear or quadratic functions for simplicity. For example, [2] assumed a constant thermal efficiency for a gas turbine and formulated the electricity consumption of a desalination plant as a quadratic function of freshwater production rate.

This paper seeks to optimize the operations of an IES that encompasses a small modular reactor (SMR), a steam manifold, a balance of plant (BOP), a high-temperature steam electrolysis (HTSE) unit, and a DH network with thermal energy storage (TES). We develop our model based on our previous IES design featuring a cascade heat utilization design [11], which offers an efficient method of heat utilization by recovering waste heat from high-temperature processes for use in lower-temperature processes. We formulate the operations of this multi-carrier energy system as a mixed-integer linear programming (MILP) problem. Specifically, we adopt a piece-wise linear approach to approximate the nonlinear conversion processes of different energy carriers in our IES, including electricity, heat, and hydrogen, by sampling from a high-fidelity physics model. Our model maximizes net revenue from electricity and hydrogen sales while adhering to physical limits and operating constraints of all subsystems. The model's efficacy is assessed by considering fluctuating hourly electricity prices and heat demands over a 24-hour period.

The remainder of this paper is organized as follows. Section II formulates the exact nonlinear models of subsystems in the nuclear-based IES. We propose a linear formulation of DH in Section III. The MILP formulation for IES operation is presented in Section IV. Section V tests the proposed MILP model numerically. Section VI concludes.

II. System Modeling

The configuration of the IES depicted in Fig. 1 features a comprehensive network of six subsystems: an SMR, a steam manifold, a BOP, an HTSE unit, a DH system, and an electrical grid. The SMR generates heat that subsequently produces high-temperature steam in a steam generator. The steam is channeled to HTSE, DH, and BOP through the steam manifold. The electricity generated by the BOP can be either consumed by HTSE or sold to the electrical grid. A more detailed description of the IES can be found in [11]. This section provides a detailed modeling for each subsystem.

A. Steam Manifold

SMR functions as the primary energy source for the IES, utilizing nuclear fission to generate the high temperature steam. The steam manifold then distributes the high temperature steam from the steam generator to HTSE, BOP, and DH. Its operation is subject to the mass flow balance constraint, as expressed by:

$$\dot{m}_t^{HTSE} + \dot{m}_t^{DH} + \dot{m}_t^{BOP} = \dot{m}_t^{CS}. \qquad (1)$$
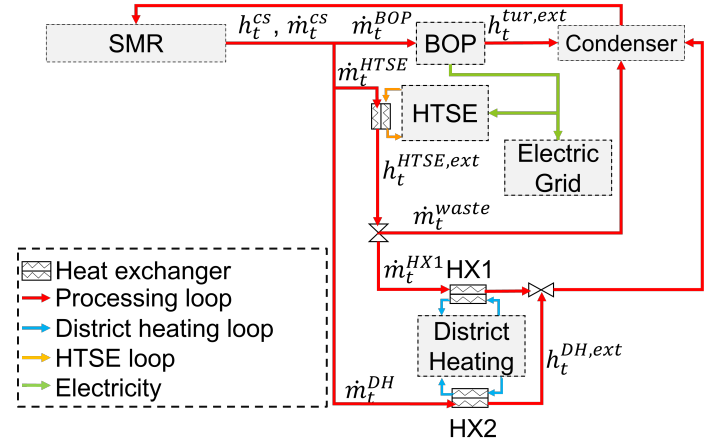

Fig. 1: Mass and energy flow in IES. Directed arrows represent mass and energy flow. The HTSE and DH subsystems are equipped with heat exchangers (HX1 and HX2) to transfer heat from the SMR's secondary coolant for downstream use without mass exchange.

B. High-temperature Steam Electrolysis (HTSE)

HTSE utilizes both heat and electricity to split water into hydrogen and oxygen. Within the IES, heat is sourced from high-temperature steam, represented by m_t^{HTSE}, directly extracted from the steam generator of SMR. The required electricity, denoted by p_t^{HTSE}, is either produced by synchronous generators or purchased from the electrical grid. The electricity consumption and the steam mass flow rate can be described by a nonlinear function in terms of hydrogen production rate, $m_t^{H_2}$. To make our model more computationally tractable, we approximate the nonlinear relationship between p_t^{HTSE} and $m_t^{H_2}$ using a linear function

$$p_t^{HTSE} = b_0 + k_0 \cdot \dot{m}^{H_2} \qquad (2)$$

where the coefficient and constant are determined via linear regression. This regression utilizes sample data pairs $(p_t^{HTSE}, m_t^{H_2})$ generated from a high-fidelity physics-based model [14]. Similarly, m_t^{HTSE} can also be linearly approximated in terms of $m_t^{H_2}$ as:

$$\dot{m}_t^{HTSE} = b_1 + k_1 \cdot \dot{m}_t^{H_2}. \qquad (3)$$

Under rated capacity, the HTSE can produce hydrogen at 0.4 kg/s. In this paper, we focus on the operating range of the mass flow rate: 0.1606 kg/s $\leq \dot{m}_t^{H_2} \leq$ 0.3977 kg/s. Within this range, (2) and (3) effectively represent p_t^{HTSE} and $m_t^{H_2}$ in terms of $\dot{m}_t^{H_2}$, respectively. Beyond this range, the physics-based model shows highly nonlinear behaviors. The coefficients of the regression models in (2) and (3) are presented in Table I. The r-squared values for the models in (2) and (3) are 0.9971 and 0.9948, respectively.

C. District Heating Network

The DH system extracts heat from HTSE exhaust or reactor process steam to meet end-use heat demands. As depicted in

TABLE I: Coefficients of the linearized HTSE Model.

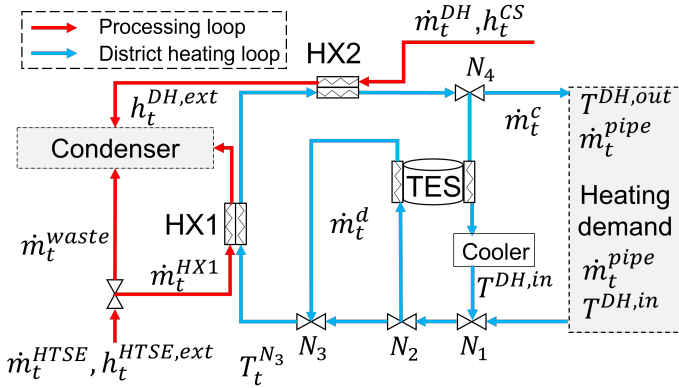| b_0 (kW)	k_0 (We·s/g)	b_1 (kg/s)	k_1
5.502×10^3	1.212×10^5	1.1947	18.2765

Fig. 2: Mass and energy flow in the DH network. The network has 4 nodes, N_1 to N_4, where flow conservation is enforced. The supply temperature $T^{DH,out}$ and the return temperature $T^{DH,in}$ are maintained at constants values. The cooler in the TES charging line removes unused heat from the charging flow to lower the temperature to $T^{DH,in}$. The temperature of the merged flow at node N_1 remains constant at $T^{DH,in}$.

Fig. 2, the DH system consists of two heat exchangers (HX1 and HX2), a sensible TES system, and a network of pipelines. HX1 recovers heat from the HTSE exhaust. If the heat from the HTSE exhaust exceeds the DH demand, a bypass line redirects the excess heat to a condenser. The steam mass flow rate in HX1 is therefore bound by the available steam in the HTSE:

$$\dot{m}_t^{HX1} \leq \dot{m}_t^{HTSE}. \tag{4}$$

When the heat from HTSE is insufficient for the demand, additional heat is extracted by HX2 from the reactor process steam. Assuming no heat loss in the environment, we calculate the heat supplied by HX1 and HX2 as follows:

$$q_t^{HX1} = \dot{m}_t^{HX1}(h_t^{HTSE,ext} - h^{DH,ext}) \tag{5}$$

$$q_t^{HX2} = \dot{m}_t^{DH}(h^{CS} - h^{DH,ext}) \tag{6}$$

TES stores and releases heat to balance between supply and demand. In our system, heat is stored in the form of hot water. Note that we assume a homogeneous distribution of temperature in the TES and both the charging and discharging flows are in thermodynamic equilibrium with the TES before they exit the TES. During the charging cycle, a portion of hot water, denoted by $\dot{m}_t^c$, exits HX2 at temperature $T^{DH,out}$ and enters the TES. After releasing its heat, the water returns at temperature T_t^{TES}. The cooler further brings down the temperature of this returning flow to $T^{DH,in}$. In the discharging phase, a fraction of feed water, represented by $\dot{m}_t^d$, is directed to the TES at node N_2 with a temperature of $T^{DH,in}$. This preheated water returns at temperature T_t^{TES} and then merges

with the remaining feed water at node N_3 before entering HX1. The average temperature of TES can be formulated as:

$$T_t^{TES} = T_{t-1}^{TES} + \frac{c_p \Delta t}{c_{str} m_{str}}[\dot{m}_t^c(T^{DH,out} - T_t^{TES})$$
$$- \dot{m}_t^d(T_t^{TES} - T_t^{D,in})]. \tag{7}$$

The lower and upper bounds of T_t^{TES} are given by:

$$T_{min}^{TES} \leq T_t^{TES} \leq T_{max}^{TES}. \tag{8}$$

The lower and upper bounds of the charging and discharging flow rates are:

$$0 \leq \dot{m}_t^c \leq \dot{m}_{max}^c, 0 \leq \dot{m}_t^d \leq \dot{m}_{max}^d. \tag{9}$$

The resulting temperatures in the DH network, following the heating process of TES and heat exchangers, are respectively described by the following equations:

$$T_t^{N_3} = \frac{(\dot{m}_t^{pipe} + \dot{m}_t^c - \dot{m}_t^d)T^{DH,in} + \dot{m}_t^d T_t^{TES}}{(\dot{m}_t^{pipe} + \dot{m}^c)}, \tag{10}$$

$$T^{DH,out} = T_t^{N_3} + \frac{q_t^{HX1} + q_t^{HX2}}{c_p(\dot{m}_t^{pipe} + \dot{m}_t^c)}. \tag{11}$$

D. Balance of Plant

The BOP includes a steam turbine and a synchronous generator. In addition, a turbine valve regulates the steam flow to the steam turbine, with any excess steam rerouted to the condenser via a bypass valve. The mass balance equation in the BOP is given by:

$$\dot{m}_t^{BOP} = \dot{m}_t^{BV} + \dot{m}_t^{Tur}. \tag{12}$$

The steam turbine converts heat into mechanical power:

$$p_t^{mech} = \eta_t \dot{m}_t^{Tur}(h^{CS} - h_t^{Tur,ext}). \tag{13}$$

The mechanical power is further converted into electrical power by a synchronous generator:

$$p_t^g = \eta_g p_t^{mech}. \tag{14}$$

For utility-scale units, η_t and η_g typically exceed 90% [15] and 95% [16], respectively.

E. Electrical Grid

The mismatch between the electricity demand of the HTSE, p_t^{HTSE}, and the electricity production of the synchronous generator, p_t^g, is balanced by either selling (p_t^s) electricity to or buying (p_t^b) from the grid:

$$p_t^s + p_t^{HTSE} = p_t^g + p_t^b. \tag{15}$$

III. LINEAR MODEL OF DISTRICT HEATING NETWORK

The above system models provide a mathematical description of operations of the IES, and our objective is to find the most cost-efficient operating schedules subject to these constraints. Directly enforcing these constraints, however, will lead to a nonlinear optimization model, because of existence of several nonlinear constraints (e.g., (5), (7), (10), and (11)). These nonlinear constraints are used to model thermodynamics of the DH system, and consist of products of two decision variables. This section therefore focuses on the linearization of these constraints to make our model mathematically tractable.

A. Linearize the Product of TES's Charging/discharging Flow and Temperature

To linearize the products of two continuous variables (e.g., $\dot{m}_t^c T_t^{TES}$ and $\dot{m}_t^d T_t^{TES}$ in (7), (10), and (11)), we adopt a 2-step binary formulation. We start by linearizing $\dot{m}_t^c T_t^{TES}$ from (7). First, we discretize the charging flow rate using n binary variables, $\lambda_{i,t}^c$, expressed as:

$$\lambda_{i,t}^c \in \{0,1\}, \forall i \in \{0,1,...,n-1\}, \tag{16}$$

$$\sum_{i=0}^{n-1} \lambda_{i,t}^c = 1, \tag{17}$$

$$\dot{m}_t^c = \sum_{i=0}^{n-1} i \frac{\dot{m}_{max}^c}{n} \lambda_{i,t}^c. \tag{18}$$

Note that (18) approximates the continuous variable $\dot{m}_t^c$ with n segments. Consequently, the nonlinear product is converted into a sum of products, each consisting of a continuous variable multiplied by a constant and a binary variable:

$$\dot{m}_t^c T_t^{TES} = \frac{\dot{m}_{max}^c}{n} \sum_{i=0}^{n-1} i(\lambda_{i,t}^c T_t^{TES}). \tag{19}$$

Next, each discretized product $\lambda_{i,t}^c T_t^{TES}$ is further reformulated into a linear form by introducing a new variable, $y_{i,t}^{cTES}$:

$$\lambda_{i,t}^c T_{min}^{TES} \leq y_{i,t}^{cTES} \leq \lambda_{i,t}^c T_{max}^{TES}, \tag{20}$$

$$\sum_{i=0}^{n-1} y_{i,t}^{cTES} = T_t^{TES}, \tag{21}$$

$$\dot{m}_t^c T_t^{TES} = \sum_{i=0}^{n-1} i \frac{\dot{m}_{max}^c}{n} y_{i,t}^{cTES}. \tag{22}$$

Similarly, $\dot{m}_{i,t}^d T_t^{TES}$ in (10) can be reformulated into:

$$\lambda_{i,t}^d \in \{0,1\}, \forall i \in \{0,1,...,n-1\}, \tag{23}$$

$$\sum_{i=0}^{n-1} \lambda_{i,t}^d = 1, \tag{24}$$

$$\lambda_{i,t}^d T_{min}^{TES} \leq y_{i,t}^{dTES} \leq \lambda_{i,t}^d T_{max}^{TES}, \tag{25}$$

$$\sum_{i=0}^{n-1} y_{i,t}^{dTES} = T_t^{TES}, \tag{26}$$

$$\dot{m}_t^d T_t^{TES} = \sum_{i=0}^{n-1} i \frac{\dot{m}_{max}^d}{n} y_{i,t}^{dTES}. \tag{27}$$

B. Linearize the Thermal Power Extracted by HX1

In (5), $\dot{m}_t^{HX1}$ is a continuous variable, whereas $h_t^{HTSE,ext}$ is a nonlinear function of the hydrogen production rate, $\dot{m}_t^{H_2}$. We therefore linearize (5) as follows.

First, we approximate $h_t^{HTSE,ext}$ as a piece-wise constant function of $\dot{m}_t^{H_2}$:

$$h_t^{HTSE,ext} = \begin{cases} h_0, & a_0 \leq \dot{m}_t^{H_2} \leq a_1 \\ h_1, & a_1 < \dot{m}_t^{H_2} \leq a_2 \\ \vdots & \\ h_{k-1}, & a_{k-1} < \dot{m}_t^{H_2} \leq a_k \end{cases}. \tag{28}$$

TABLE II: Coefficients of the linearized DH model, where k denotes the number of segments. Units: a_0 to a_9: kg/s, h_0 to h_8: 10^3 kJ/kg.

k	a_0	a_1	a_2	a_3	a_4	a_5
9	0.161	0.187	0.213	0.24	0.266	0.292

a_6	a_7	a_8	a_9	h_0	h_1	h_2
0.319	0.345	0.371	0.398	1.408	1.366	1.340

h_3	h_4	h_5	h_6	h_7	h_8
1.315	1.303	1.306	1.310	1.320	1.339

The breakpoints a_i's are evenly distributed and the function's values h_i's are determined via ordinary least squares regression, based on the sample set $(\dot{m}_t^{H_2}, h_t^{HTSE,ext})$ produced from the same high-fidelity physics-based model as in Section II-B. The parameters for the regression model are presented in Table II, resulting in an r-squared value of 0.9529. Eq. (28) can be expressed with k binary variables, λ_i:

$$\lambda_{i,t} \in \{0,1\}, \forall i \in \{0,1,...,k-1\}, \tag{29}$$

$$\sum_{i=0}^{k-1} \lambda_{i,t} = 1, \tag{30}$$

$$\sum_{i=1}^{k-1} a_i \lambda_{i,t} < \dot{m}_t^{H_2} \leq \sum_{i=0}^{k-1} a_{i+1} \lambda_{i,t}, \tag{31}$$

$$h_t^{HTSE,ext} = \sum_{i=0}^{k-1} h_i \lambda_{i,t}. \tag{32}$$

From the above, the nonlinear term $\dot{m}_t^{HX1} h_t^{HTSE,ext}$ is transformed into a sum of products, each multiplying $\dot{m}_t^{HX1}$ by a constant and a binary variable:

$$\dot{m}_t^{HX1} h_t^{HTSE,ext} = \sum_{i=0}^{k-1} h_i(\dot{m}_t^{HX1} \lambda_{i,t}). \tag{33}$$

Next, each product $(\dot{m}_t^{HX1} \lambda_{i,t})$ is equivalently converted into a linear form by introducing a new variable, $y_{i,t}^{HX1}$:

$$\lambda_{i,t} \dot{m}_{min}^{HX1} \leq y_{i,t}^{HX1} \leq \lambda_{i,t} \dot{m}_{max}^{HX1}, \forall i \in \{0,1,...,k-1\}, \tag{34}$$

$$\sum_{i=0}^{k-1} y_{i,t}^{HX1} = \dot{m}_t^{HX1}, \tag{35}$$

$$\dot{m}_t^{HX1} h_t^{HTSE,ext} = \sum_{i=0}^{k-1} h_i y_{i,t}^{HX1}. \tag{36}$$

Finally, the entire reformulation of (5) is given by:

$$q_t^{HX1} = \sum_{i=0}^{k-1} h_i y_{i,t}^{HX1} - \dot{m}_t^{HX1} h^{DH,ext}. \tag{37}$$

IV. MODEL FORMULATION

The operations of IES can be modeled as a mixed-integer linear programming (MILP) problem. The model maximizes net revenue from sales of electricity and hydrogen minus costs

TABLE III: Additional parameters of the scheduling model.

$c^{str/p}$ (kJ/(kg·K))	T_{max}^{TES} (°C)	m^{str} (kg)	n
4.2	98	10^6	14
$h^{Tur,ext}$ (kJ/kg)	T_{min}^{TES} (°C)	$\dot{m}_{max}^c$ (kg/s)	η_t
2364.388	60	10	0.9
$h^{DH,ext}$ (kJ/kg)	$T^{DH,out}$ (°C)	$\dot{m}_{max}^d$ (kg/s)	η_g
699.30	90	10	0.95
h^{CS} (kJ/kg)	$T^{DH,in}$ (°C)	$\dot{m}^{CS}$ (kg/s)	Δt (seconds)
3010.93	40	84	3600

of purchasing electricity. Simultaneously, it ensures compliance with the physical constraints of all the subsystems, operating under the rated reactor power condition. The problem formulation is given as:

$$\max \Delta t \sum_{t=1}^{T} \left[a_{1,t} \times \frac{(p_t^s - p_t^b)}{3600} + a_{2,t} \times \dot{m}_t^{H_2} \right],$$
$$\text{s.t. } (1)-(4),(6),(8),(9),(16)-(18),(20)-(27)$$
$$(29)-(31),(34),(35),(37). \tag{38}$$

where $a_{1,t}$ and $a_{2,t}$ denote the price of electricity and hydrogen at time t, respectively. T represents the scheduling horizon.

V. CASE STUDY

In this section, we aim to analyze the economic operation of IES using the proposed model. The goal is to meet heating demands while maximizing total revenues.

A. Simulation Setup

To analyze the economic performance of the IES, we simulated a scenario based on a 24-hour heating demand profile, as depicted in the top panel of Fig. 5. Throughout the simulation, the SMR maintained a constant thermal power generation at its rated capacity, resulting in constant values for both the flow rate ($\dot{m}^{CS}$) and enthalpy (h^{CS}) of the steam delivered from SMR, along with the enthaply of steam exiting turbine ($h^{Tur,ext}$). The IES participates in the DA energy market by either buying or selling electricity. The 24-hour DA electricity prices were collected at node HOLM1 on July 1st, 2021 from CAISO [17] (Fig. 3). The hydrogen price was assumed to be 1.8 \$/kg [7], [18]. The initial temperature of TES is 60 °C. Additional parameters in the scheduling model (38) are provided in Table III. We implemented this model in Python using Pyomo, and used CPLEX to solve it on a laptop with 8 cores and 16 GB of memory in 16.6 seconds.

B. Simulation Results

1) Economic Performance: Fig. 3 presents the electricity prices, which are notably high between hours 16 and 20. In response to the fluctuating prices, the top panel of Fig. 4 illustrates the IES' strategy: selling electricity during peak periods and purchasing electricity for hydrogen production during off-peak periods, as reflected by positive electricity sales when electricity prices are high and positive electricity procurement otherwise. In addition, the panel highlights the

electricity balance. The power output of turbine surpasses HTSE's consumption between hours 16 and 20, with the surplus sold to the grid. When the HTSE's electricity demand exceeds the turbine's generation, the deficit is addressed by the purchased electricity. This operating strategy is also reflected in the dispatch schedules of steam. As shown in the middle panel of Fig. 4, more steam is directed to BOP during peak periods for electricity generation and the steam flow rate in the HTSE is reduced to its lower bound, which results in a reduced hydrogen production rate.
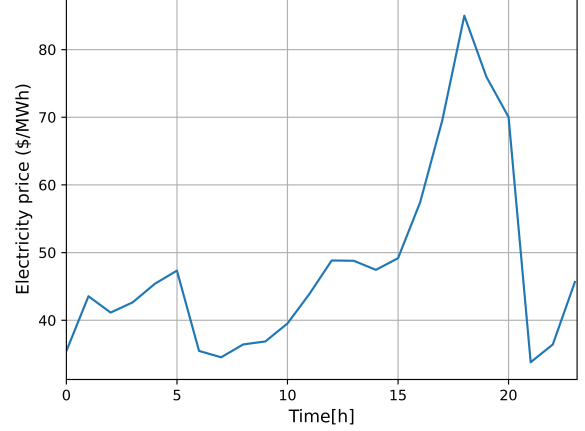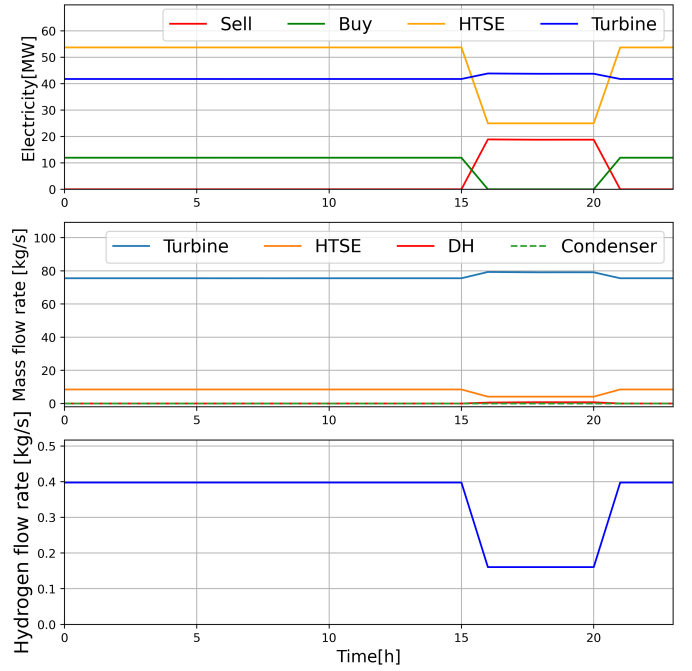

Fig. 3: 24-hour DA electricity price. Source: [17].

Fig. 4: Operating schedules of the IES over a 24-hour period. **Top:** Electricity generated by BOP (Turbine), consumed by HTSE, sold to (Sell) and bought from (Buy) the grid. **Middle:** Flow rates of steam supplied by steam manifold to HTSE, DH, Turbine, and condenser. **Bottom:** Hydrogen production rate.

2) Heat Demand-Supply Balance: Fig. 5 shows the heat demand-supply balance of the IES and benefits of cascade heat utilization. Heat demand is relatively low during hours 0-4, 8-15, and 21-23, and the heat recovered from the HTSE exhaust alone can meet the demand. The excess heat is stored by the TES, as depicted in the middle panel. When the HTSE exhaust heat is inadequate, the deficit is compensated by discharging the TES, which is especially evident between hours 5 and 8. Between hours 16 and 20, even discharging the TES is insufficient to bridge the gap, therefore, additional topping heat is extracted directly from SMR. Our results suggest that the TES temperature fluctuates within the operation range between 60 and 98°C throughout the simulated period. The temperature increases during low-demand periods and decreases during high-demand periods, consistent with the charging and discharging schedules of the TES.

Our simulation highlights the effectiveness of the cascaded heat design: The recovered heat from the HTSE exhaust is sufficient to meet the DH demand most of the time, significantly improving system efficiency and cost-effectiveness.
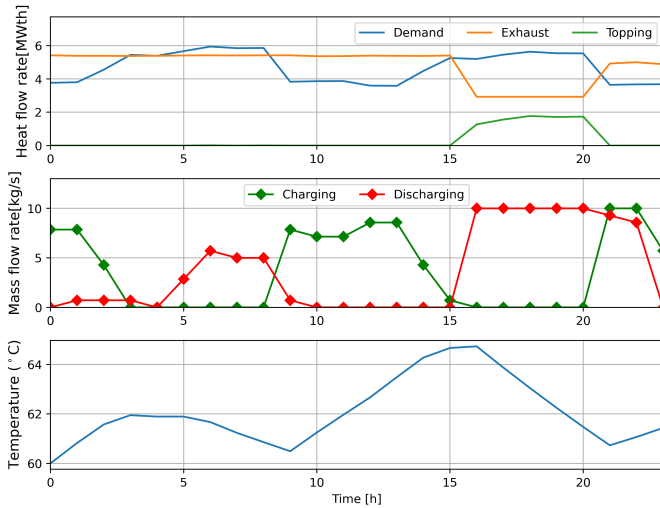

Fig. 5: Heat demand-supply dynamics in the IES over a 24-hour period. **Top:** Comparison of the DH demand (Demand) with heat supplied by the HTSE exhaust (Exhaust) and the process steam (Topping). **Middle:** Charging and discharging flow rates of the TES. **Bottom:** Temperature profile of the TES.

VI. CONCLUSION

This paper developed an MILP framework for the optimal dispatch of a nuclear-based IES encompassing an SMR, a steam manifold, a BOP, an HTSE, a DH system, and an electrical grid. Assuming the SMR operates at rated reactor power condition, we carried out 24-hour numerical simulations with varying heat demand in a wholesale electricity market. The numerical results validate the efficacy of the proposed model by demonstrating its capability to meet heat demand requirements throughout the simulation. Moreover, the model maximizes revenue by selling electricity during peak periods and purchasing electricity for hydrogen production during off-peak periods.

In the future, we will extend our scope by incorporating more components in the IES, such as renewable energy resources and other industrial processes. We will also examine the impact of fluctuating energy prices on the optimal operating schedules.

REFERENCES

[1] M. F. Ruth *et al.*, "Nuclear-renewable hybrid energy systems: Opportunities, interconnections, and needs," *Energy Convers. Manag.*, vol. 78, pp. 684–694, 2014.
[2] J. Chen *et al.*, "Operations optimization of nuclear hybrid energy systems," *Nuclear Technology*, vol. 195, no. 2, pp. 143–156, 2016.
[3] J. S. Kim *et al.*, "Dynamic performance analysis of a high-temperature steam electrolysis plant integrated within nuclear-renewable hybrid energy systems," *Applied energy*, vol. 228, pp. 2090–2110, 2018.
[4] B. Poudel and R. Gokaraju, "Optimal operation of SMR-RES hybrid energy system for electricity & district heating," *IEEE Trans. Energy Convers.*, vol. 36, no. 4, pp. 3146–3155, 2021.
[5] W. Dazhong, M. Changwen, D. Duo, and L. Jiagui, "Chinese nuclear heating test reactor and demonstration plant," *Nuclear Engineering and Design*, vol. 136, no. 1-2, pp. 91–98, 1992.
[6] B. Poudel and R. Gokaraju, "Small modular reactor (SMR) based hybrid energy system for electricity & district heating," *IEEE Trans. Energy Convers.*, vol. 36, no. 4, pp. 2794–2802, 2021.
[7] Z. Yi *et al.*, "Deep reinforcement learning based optimization for a tightly coupled nuclear renewable integrated energy system," *Applied Energy*, vol. 328, p. 120113, 2022.
[8] A. Basit *et al.*, "Efficient and autonomous energy management techniques for the future smart homes," *IEEE Trans. Smart Grid*, vol. 8, no. 2, pp. 917–926, 2017.
[9] M. Bozchalui *et al.*, "Optimal operation of residential energy hubs in smart grids," *IEEE Trans. Smart Grid*, vol. 3, no. 4, pp. 1755–1766, 2012.
[10] B. F. Hobbs *et al.*, *The next generation of electric power unit commitment models*. Springer Science & Business Media, 2006, vol. 36.
[11] B. Poudel *et al.*, "Design, modeling and simulation of nuclear-powered integrated energy systems with cascaded heating applications," *J. Renew. Sustain. Energy*, vol. 15, no. 5, 2023.
[12] R. A. Jacob and J. Zhang, "Modeling and control of nuclear–renewable integrated energy systems: Dynamic system model for green electricity and hydrogen production," *J. Renew. Sustain. Energy*, vol. 15, no. 4, 2023.
[13] J. Rahman and J. Zhang, "Multi-timescale operations of nuclear-renewable hybrid energy systems for reserve and thermal product provision," *J. Renew. Sustain. Energy*, vol. 15, no. 2, 2023.
[14] Idaho National Laboratory, "Hybrid Systems Modeling and Simulation," https://github.com/idaholab/HYBRID/wiki, 2017.
[15] K. Darrow *et al.*, "Catalog of chp technologies," U.S. Environmental Protection Agency, Tech. Rep., 2015.
[16] H. E. Jordan, *Energy-efficient electric motors and their applications*. Springer Science & Business Media, 1994.
[17] CAISO, http://oasis.caiso.com/mrioasis/logon.do, accessed on: 2023-06-19.
[18] K. L. Frick *et al.*, "Evaluation of hydrogen production feasibility for a light water reactor in the midwest," Idaho National Lab.(INL), Idaho Falls, ID (United States), Tech. Rep., 2019.